

## Tunnel effects on road efficiency and travel time explored by a three lane traffic model

Zejing Hu<sup>a,c</sup>, M.N. Smirnova<sup>b,\*</sup>, Yongliang Zhang<sup>a</sup>, Zuojin Zhu<sup>a,b,\*\*</sup>, N.N. Smirnov<sup>b</sup>

<sup>a</sup> Faculty of Engineering Science, CAS Key Laboratory of Mechanical Behavior and Design Materials, University of Science and Technology of China, Hefei, 230026, China

<sup>b</sup> Faculty of Mechanics and Mathematics, Lomonosov Moscow State University, Moscow, 119992, Russia

<sup>c</sup> Anhui Xiang Shui Jian Pumped Storage Co., LTD, Wuhu 241083, China

### ARTICLE INFO

#### Keywords:

Tunnel effects  
Road efficiency  
Travel time  
Three lane traffic model  
Weighted essentially non-oscillatory scheme

### ABSTRACT

To ascertain tunnel effects upon road efficiency and travel time of ring road traffic, a mathematical model accounting of three lanes is investigated. The model uses traffic pressure and sound speed in algebraic form, and a single traffic speed to describe the vehicular motions on the three lane instantaneously to simplify mathematical modeling of traffic flow. The ring road with a total length 100 km has a tunnel with a length of 8 km and a speed limit of 80 km/h. The free flow speeds on lane I, II and III are assumed to be 110, 100, and 90 km/h. Using the model, a code is elaborated for numerical simulations on the three lane ring road. For validating the model the tunnel length is reset as 1.5 km, so that the conformity between the predicted time averaged speed and the recorded speed near the Kobotoke tunnel in Japan can be seen clearly. It is found that the threshold of traffic shock formation near the tunnel can be determined by observing spatiotemporal pattern of traffic flow. When and where traffic shock appears relies on the free flow speed on lane III. Road efficiency and travel time for the ring road traffic are predicted and discussed. The numerical findings in this paper deepen the understanding of tunnel effects.

### 1. Introduction

Many investigations for bottleneck effects of sags and freeway tunnels have been carried out as reported briefly (Zhang, et al. 2021a), some conclusions can be found in Refs (Goñi-Ros et al. 2014, 2016; Jin, 2018).

A review of the studies of multi-lane vehicular flow indicates that some very general model involving vehicular flow on a two lane homogeneous road in statistical equilibrium was introduced by Haight (1963), it was found only when the assumptions are most stringent is it possible to solve a few problems, and even then the formulas are rather formidable. After considerations for multilane traffic flow dynamics reported by Michalopoulos et al.(1984), a multi-lane model was developed by Chang and Zhu (2006) for analyzing the dynamic traffic properties of a highway segment under a lane-closure operation that often incurs complex interactions between mandatory lane-changing vehicles and traffic at unblocked lanes. For homogeneous multi-lane freeways, a macroscopic behavior theory of traffic dynamics was proposed by Daganzo (2002a), the theory was described in its

fully complexity without calculus, shown to be qualitatively consistent with experimental observations, including puzzling. Building on the continuum macroscopic behavior theory and focusing on the onset of congestion, the behavior of multi-lane freeway traffic past on ramps was further examined (Daganzo, 2002b). A multi-lane traffic model was proposed by Smirnova et al.(2014b), where an expression of the parameter for describing the acceleration component in the orthogonal direction in relation to lane changing.

The objective of this paper is to numerically ascertain the tunnel effects on road efficiency and travel time through a ring freeway with a total length of 100 km. As freeway segment with three lanes is common in the real world, a three lane traffic model (TLM) is developed. For instance, the paper assumes that the freeway has three lanes (I, II and III) whose free flow speeds are 110, 100, and 90 km/h, and a tunnel with a length of 8 km and a tunnel speed limit of 80 km/h. TLM assumes that the free flow speed in the tunnel is just the tunnel speed limit, which is used to determine the fundamental diagram (FD) with second critical speed and relevant braking distance (Kiselev, et al. 2000), as

\* Corresponding author.

\*\* Corresponding author at: Faculty of Engineering Science, CAS Key Laboratory of Mechanical Behavior and Design Materials, University of Science and Technology of China, Hefei, 230026, China.

E-mail addresses: [wonrims@inbox.ru](mailto:wonrims@inbox.ru) (M.N. Smirnova), [zuojin@ustc.edu.cn](mailto:zuojin@ustc.edu.cn) (Z. Zhu).

<https://doi.org/10.1016/j.trip.2022.100573>

Received 3 September 2021; Received in revised form 25 February 2022; Accepted 26 February 2022

Available online 28 March 2022

2590-1982/© 2022 The Author(s). Published by Elsevier Ltd. This is an open access article under the CC BY-NC-ND license (<http://creativecommons.org/licenses/by-nc-nd/4.0/>).

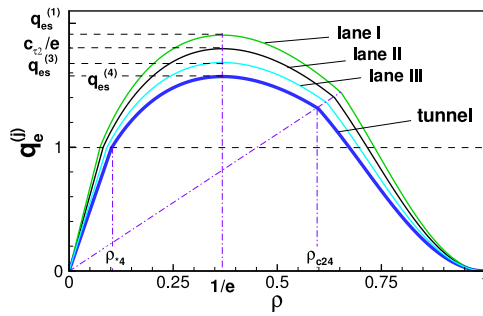


Fig. 1. Fundamental diagram (FD) for three lane traffic flows. Note that  $\rho$  is in the unit of  $\rho_m$ ,  $q_e^{(j)}$  is measured by  $q_0 (= \rho_m v_0)$ , and  $q_{es}^{(j)} = c_{e_j}/e \cdot [\rho_{e_j} v_{f_j} / \rho_{e_2} v_{f_2}]$ ,  $j = 1, 2, 3$  and 4 respectively for equilibrium flow rates on the three lanes in normal road segment, and equilibrium flow rate on any lane in the tunnel.

shown in Fig. 1, and adopts a single traffic speed to describe the vehicular streams on three lanes, and utilize traffic pressure and sound speed in algebraic form rather than partial differential equation as reported (Helbing and Treiber, 1998; Hoogendoorn and Bovy, 2000).

TLM assumes that traffic sound speed remains a constant when traffic density is above the second critical density, otherwise the sound speed has a form that can be given by the approach reported previously (Zhang et al. 2018b). Then, using the definition of sound speed in classical mechanics at constant entropy, traffic pressure can be obtained. There are different possible choices for traffic pressure and it is reasonable to allow flexibility in the description, as reported previously (Zhang, Wong and Dai, 2009), because traffic flow is a self-driven, many-particle system that is very complex (Helbing, 2001), which means that a given choice for the pressure may be suitable in one situation but not in another. However, TLM has not account for the variations of vehicular engine types, and the effects of lane width, shoulder width, and traffic accidents.

In this paper, road efficiency and travel time are selected as indicators to reflect the operational performance of the ring freeway with a tunnel. Road efficiency is predicted using the definition reported (Chen, et al. 2001; Morris and Trivedi, 2007). Travel time is estimated using the grid speed of traffic flow, which is different from the published work (Chang and Mahmassani, 1988; Wang et al. 2016). Chang and Mahmassani (1988) proposed the rules for describing urban commuters' predictions of travel time as well as the adjustments of departure time in response to unacceptable arrivals in their daily commute under limited information, while Wang, et al.(2016) predicted travel time with a regression model.

Indeed, TLM is not a full multilane macroscopic model as there is only an effective speed instead of different traffic speed on each lane, but can be seen as an extension of the double lane traffic model reported recently (Zhang, et al. 2021a). The model complexity of TLM is lower than that developed by Helbing and Greiner (1997). It is noted that the TLM application to other real-world tunnels requires a change of simulation conditions. The needs such as to model different lane configurations, the influences of lane widths and shoulder widths indicate that there are more investigations to be done in the future.

To solve TLM equations numerically, RK3 (a 3rd-order Runge–Kutta scheme) (Shu, 1988; Shu and Osher, 1989) is used to resolve the terms with time derivatives, and WENO5 (a 5th-order weighted essentially non-oscillatory scheme) (Jiang and Shu, 1996; Henrick, et al. 2005) is used to predict numerical flux. To compare the reliability and feasibility of TLM, the Navier–Stokes like model (Zhang, 2003) called as Extended Zhang's Model (EZM) (see Section 5.2) is used to provide counterpart results. The reason of selecting EZM is that the viscous model of Zhang (2003) contains practically every well-known continuum model, has a stable wave structure of first- and second-order waves, and controls the extent of non-anisotropic and diffusive influences through

a dimensionless parameter. For validating the model, the tunnel length is reset as 1.5 km so that the conformity between the predicted time averaged speed and the recorded speed near the Kobotoke tunnel in Japan (Koshi, et al. 1992) can be observed clearly. Note that this resetting of tunnel length is made similar to the work of Jin (2018).

In order to simulate vehicular flows on ring freeway with a tunnel, the equations of TLM are solved with the reliable WENO5-RK3 scheme, numerical results reveal that the threshold of traffic shock formation at the tunnel entrance can be determined by observing spatiotemporal pattern of traffic flow. Such a threshold depends on the free flow speed on lane III. The distributions of mean road efficiency and its root mean square value rely intimately on the spatiotemporal evolution of traffic flow. The tunnel with a length of 8 km provides a smooth downstream segment close to tunnel exit when there is a traffic shock occurs at tunnel entrance. Using linear regression after logarithmic processing, the mean travel time through the ring freeway with the tunnel having a length of 8 km can be fitted in a power law form.

This paper is organized as follows. In Section 2, TLM equations are presented. In Section 3, the numerical method for the solution of TLM equations is given, with the approach of estimation for travel time and road efficiency in Section 4. In Section 5, extensive numerical results are discussed. Finally, some conclusions are provided in Section 6.

## 2. Equations for a three lane traffic model

In the three lane traffic model, to avoid some complexity in mathematical modeling, we use a single traffic speed, traffic pressure and sound speed in algebraic form, similar to the work of Zhang et al.(2021a).

As shown in Fig. 2(a), three-lanes are labeled by I, II and III, corresponding to traffic densities denoted by  $\rho_1, \rho_2$  and  $\rho_3$ . Lane changing of vehicles is permitted, appears spontaneously to keep the local road homogeneity of traffic density. Generally vehicles on lane I have a higher free flow speed, those on lane III have a lower free flow speed, with the free flow speed of vehicles on lane II is somewhere in between. But if the vehicles are in the tunnel, the free flow speed on any lane must be equal to a tunnel speed limit. As shown in Fig. 2(b), the ring road has five initial jams at  $X_I, I = A, B, C, D, E$ , and a tunnel located between  $X_A$  and  $X_B$ . Vehicles on ramp runs into the ring road at three intersections  $X_{R1}, X_{R2}$ , and  $X_{R3}$ . Any vehicle attempts to run off the ring road should at first make lane changes and shift onto the lane III, and then leaves through the ramp.

As the description of the three lane traffic flow is similar to that of a double-lane traffic model (Zhang, et al. 2021a), using the ramp parameter  $\sigma$  and the traffic elasticity  $\gamma (= 0.68v\tau)$ , we can write the TLM equations in the form

$$\begin{cases} \rho_t + q_x &= \sigma q/l_0, \\ \rho(u_t + uu_x) &= R, \\ (\rho_k)_t + (\rho_k u)_x &= (\rho - \rho_k)/(\tau\beta_*), \text{ for } k = 1, 2. \end{cases} \quad (1)$$

where  $\rho = (\rho_1 + \rho_2 + \rho_3)/3$ , the traffic density on lane III  $\rho_3 = 3\rho - (\rho_1 + \rho_2)$ , and  $R$  satisfies (Zhu and Yang, 2013; Bogdanova, et al. 2015; Ma, et al. 2018)

$$R + [\rho\gamma(R/\rho)_x]_x = (q_e - q)/\tau - p_x + [\rho(v + v_1)u_x]_x, \quad (2)$$

$l_0$  is the length scale of traffic flow,  $v_1 = 3\gamma u_x$  is the viscosity depending on the product of elasticity and speed gradient (Zhu and Yang, 2013),  $p$  is traffic pressure,  $q_e$  is equilibrium traffic flow rate that can be calculated with respect to the fundamental diagrams in Fig. 1,  $R/\rho$  is the vehicular acceleration,  $v$  is the kinematic viscosity of traffic flows,  $\tau$  is the relaxation time of traffic flow, and  $\sigma$  is the ramp parameter predicted by random number generator with Gaussian normal distribution.

As there is different density on each lane, indicating that the equilibrium traffic flow rates  $q_{ei}$  are lane dependent, as shown in Fig. 1. Using the density fractions  $s_1 = \rho_1/(3\rho)$  and  $s_2 = \rho_2/(3\rho)$ ,  $q_e$  is calculated by

$$q_e = q_{e1}s_1 + q_{e2}s_2 + q_{e3}(1 - s_1 - s_2). \quad (3)$$

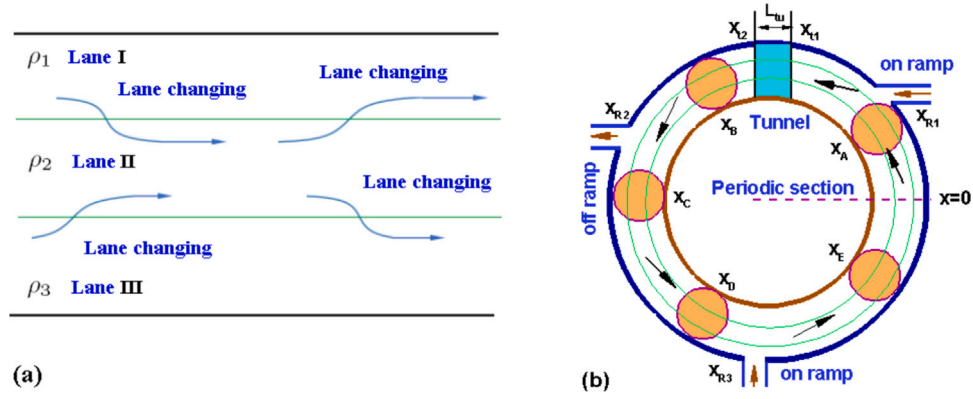


Fig. 2. (a) Three lane traffic flow, (b) Schematic of ring traffic flow with a freeway tunnel and five initial jams at  $X_I (I = A, B, C, D, E)$ . The tunnel entrance and exit are located at  $X_{tu1}$  and  $X_{tu2}$ , tunnel length  $L_{tu} = X_{tu2} - X_{tu1}$ .

Table 1  
Parameters of traffic flow on ring road.

$v_{f1}$ (km/h)	110	$\rho_{*1}$	0.0746	$X_C$ (km)	50
$v_{f2}$ (km/h)	100	$\rho_{*2}$	0.0819	$X_D$ (km)	70
$v_{f3}$ (km/h)	90	$\rho_{*3}$	0.0909	$X_E$ (km)	90
$v_{f4}$ (km/h)	80	$\rho_{*4}$	0.1021	$X_{tu1}$ (km)	20
$X_{br1}$ (m)	72	$\rho_{c21}$	0.6538	$X_{tu2}$ (km)	28
$X_{br2}$ (m)	65	$\rho_{c22}$	0.6374	$L_{tu}$ (km)	8
$X_{br3}$ (m)	58	$\rho_{c23}$	0.6190	$\rho_m$ (veh/km)	172
$X_{br4}$ (m)	51	$\rho_{c24}^a$	0.5984	$u_{c2}$ (km/h)	18
$c_{r1}(v_0)$	5.172	$X_{R1}$ (km)	12	$l$ (m)	5.8
$c_{r2}(v_0)$	4.879	$X_{R2}$ (km)	45	$l_0$ (m)	100
$c_{r3}(v_0)$	4.582	$X_{R3}$ (km)	78	$v_0 = \rho_{*2} v_{f2}$ (m/s)	2.2756
$c_{r4}(v_0)$	4.280	$\sigma_{1av}$	0.05	$t_0 = l_0/v_0$ (s)	43.9448
$A_1$	2.354	$\sigma_{2av}$	[-0.2, -0.1]	$L$ (km)	100
$A_2$	2.220	$\sigma_{3av}$	0.05	$Re = l_0 v_0 / \nu$	64
$A_3$	2.085	$X_A$ (km)	10	$\beta_*$	3
$A_4$	1.948	$X_B$ (km)	30		

<sup>a</sup>  $\rho_{*j}$  and  $\rho_{c2j}$  for  $j = 1, 2, 3, 4$  are measured by  $\rho_m$ .

In the normal segment excluding the tunnel  $x \notin [X_{tu1}, X_{tu2}]$ ,  $l \in \{1, 2, 3\}$ , let jam density be  $\rho_m$ , equilibrium traffic flow rates can be written as (Zhang et al. 2018a)

$$q_{el} = \begin{cases} \rho_l v_{f_l}, & \text{for } \rho_l \leq \rho_{*l}; \\ -c_{\tau l} \rho_l \ln(\rho_l / \rho_m), & \text{for } \rho_{*l} < \rho_l \leq \rho_{c2l}; \\ B_l \rho_l \{1 - \text{sech}[A_l \ln(\rho_l / \rho_m)]\}, & \text{for } \rho_{c2l} < \rho_l \leq \rho_m. \end{cases} \quad (4)$$

While in the tunnel  $x \in [X_{tu1}, X_{tu2}]$ , as the free flow speed is just the same as tunnel speed limit  $v_{f4}$  (see Table 1), equilibrium traffic flow rates are

$$q_{el} = \begin{cases} \rho_l v_{f4}, & \text{for } \rho_l \leq \rho_{*l}; \\ -c_{\tau 4} \rho_l \ln(\rho_l / \rho_m), & \text{for } \rho_{*l} < \rho_l \leq \rho_{c2l}; \\ B_4 \rho_l \{1 - \text{sech}[A_l \ln(\rho_l / \rho_m)]\}, & \text{for } \rho_{c2l} < \rho_l \leq \rho_m. \end{cases} \quad (5)$$

For  $j \in \{1, 2, 3, 4\}$ , in the definition of the equilibrium traffic speed at saturation state  $c_{\tau j}$ , the average length of vehicles  $l_{veh}$  has to be used. In the definition of  $B_j$ , the second critical speed  $u_{c2}$ , and the speed ratio  $A_j (= c_{\tau j} / u_{c2})$  is used, as reported by Zhang et al. (2021a).

Similar to the work of Zhang et al. (2018b), TLM employs the definition of sound speed in classical mechanics, so that traffic pressure can be expressed as  $p = c^2 \rho$ , assumes that the sound speed  $c$  is equal to the equilibrium traffic speed at saturation  $c_{\tau}$  at the second critical density  $\rho_{c2l}$ , and is inversely proportional to the relaxation time of vehicular flow. However, the vehicular types, such as electric, hybrid and fuel burning, has not been considered as an influence feature. Also, TLM has not taken the account for the variations of vehicular engine types.

The sound speed denotes velocity of weak disturbances counter flow propagation. It is determined by the signal transmission from the vehicle in front to the vehicle following behind. Imagine, the front vehicle driver applies brakes. Then the back lights begin shining, the driver of the second vehicle sees the lights (signal transmission can be considered immediate with the light speed), and then the brain and muscular signal processing and vehicle reaction on pressing the pedal gives totally the relaxation time, which is in the denominator. While in the numerator, one has the distance between the back lights of the first and second vehicles, which is the sum of distance between vehicles plus average vehicle length. It can be seen from the above analysis, that the main parameters, characterizing sound speed - the distance between the vehicles and the reaction time of a human driver - have a low dependence on the vehicle type. The vehicle characteristics could affect the vehicle length and pedal pressing response time, which is an order of magnitude smaller. This may be the scope for further research.

As the expressions of traffic pressure and sound speed are also similar to the reported (Zhang, et al. 2018b), we will also omit them. But it is worth noting that we have assumed that when traffic density is over second critical point, traffic sound speed is exactly equal to the speed  $c_{\tau j}$ , as shown in Figs. 3(a-b) for the case of  $\rho_0 = 0.25$ , where traffic sound speed ratio  $c/c_0$  and traffic pressure  $p$  in the tunnel are illustrated with legend *tunnel*, and *normal* for those in the normal segment.

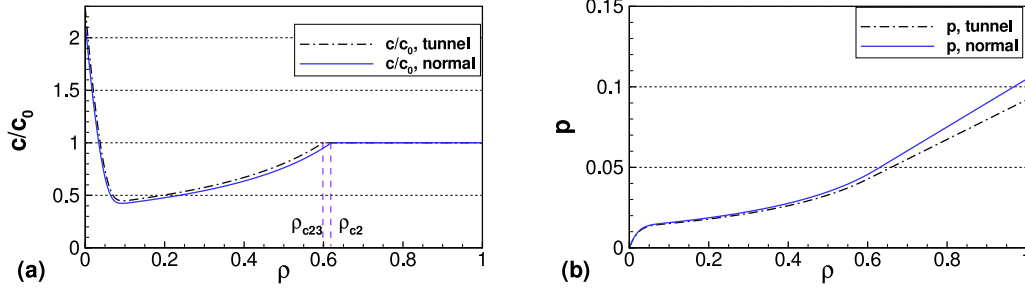


Fig. 3. Sound speed ratio  $c/c_0$  (a) and traffic pressure  $p$  (b) versus density  $\rho$  for  $\rho_0 = 0.25$ , where  $\rho$  is measured by jam density  $\rho_m$ , with  $p$  measured by  $\rho_m v_{f2}^2$ .

### 3. Numerical method

Using definition  $c^2 = \partial p / \partial \rho$ , the pressure gradient  $p_x$  may be written as

$$p_x = c^2 \rho_x,$$

then taking  $R_1 = R + p_x + \sigma q u / l_0$  instead of  $R$ , the governing Eqs. become

$$\frac{\partial \mathbf{U}}{\partial t} + \frac{\partial \mathbf{F}(\mathbf{U})}{\partial x} = \mathbf{S}, \quad (6)$$

where  $\mathbf{U} = (\rho, q, \rho_1, \rho_2)^T$ ,  $\mathbf{F}(\mathbf{U}) = (q, q^2/\rho + p, \rho_1 q/\rho, \rho_2 q/\rho)^T$ ,  $\mathbf{S} = [\sigma q/l_0, R_1, (\rho - \rho_1)/(\tau \beta_*)^T, (\rho - \rho_2)/(\tau \beta_*)^T]^T$ , superscript ' $T$ ' represents vector transpose.

The eigenvalues of Eq. (6) $a_k$ , ( $k = 1, 2, 3, 4$ ) are  $a_1 = u - c$ ,  $a_2 = u + c$ , and  $a_3 = a_4 = u$ , and the Jacobian matrix is

$$\mathbf{A} = \begin{pmatrix} 0 & 1 & 0 & 0 \\ -u^2 + c^2 & 2u & 0 & 0 \\ -\frac{uU_3}{U_1} & \frac{U_3}{U_1} & u & 0 \\ -\frac{uU_4}{U_1} & \frac{U_4}{U_1} & 0 & u \end{pmatrix}. \quad (7)$$

To solve TLM equation (6), RK3 (Shu, 1988; Shu and Osher, 1989) is used to resolve the time derivative term, and WENO5 (Jiang and Shu, 1996; Henrick, et al. 2005) is used to calculate numerical flux terms. As some detail of the numerical method has been given elsewhere (Zhang, et al. 2021a), we will not repeat it. But it is worth noting that the Courant number CFL for the Courant–Friedrichs–Lewy (CFL) condition (Shui, 1998) is assigned as 0.6 to ensure numerical stability in the numerical simulations of this paper.

### 4. Approaches for travel time and road efficiency

#### 4.1. Approach for travel time

Using the approach presented by Zhang et al. (2018a), we can estimate the local average speed  $\bar{u}_i(t)$  at  $x_i$ , with  $i$  depending on the segment index  $\hat{k}$ : if  $\hat{k} = 4$ , the grid  $x_i, i \in [n_{tu1}, n_{tu2}]$  is in the tunnel, else if  $\hat{k} = 3$ , the grid is in the normal road segment. The total length of ring road is

$$L = \sum_{\hat{k}=3}^4 L^{(\hat{k})}. \quad (8)$$

The instantaneous travel times through the road and tunnel may be written as

$$T_t(t) = \sum_{i=0}^{I_{\max}} \Delta x_i / \bar{u}_i(t), \quad T_{tu,t}(t) = \sum_{i=n_{tu1}}^{n_{tu2}} \Delta x_i / \bar{u}_i(t). \quad (9)$$

Using time averaging, labeling the time of simulation start by  $t_{st}$  and the time of simulation end by  $t_{end}$ , the mean travel time through the

road, and the tunnel mean travel time  $T_{tu,av}$  are

$$\begin{cases} T_{t,av} = \frac{1}{t_{end} - t_{st}} \int_{t_{st}}^{t_{end}} T_t(\xi) d\xi, \\ T_{tu,av} = \frac{1}{t_{end} - t_{st}} \int_{t_{st}}^{t_{end}} T_{tu,t}(\xi) d\xi. \end{cases} \quad (10)$$

with the rms values  $T_t'$  and  $T_{tu}'$  given by

$$\begin{cases} T_t' = \left\{ \frac{1}{t_{end} - t_{st}} \int_{t_{st}}^{t_{end}} [T_t(\xi) - T_{t,av}]^2 d\xi \right\}^{1/2}, \\ T_{tu}' = \left\{ \frac{1}{t_{end} - t_{st}} \int_{t_{st}}^{t_{end}} [T_{tu,t}(\xi) - T_{tu,av}]^2 d\xi \right\}^{1/2}. \end{cases} \quad (11)$$

#### 4.2. Approach for road efficiency

Road efficiency is also a crucial indicator for traffic flow dynamics, as traffic congestion is not caused by demand exceeding capacity but because of inefficient operation of highways during periods of peak demand (Chen, et al. 2001). With the definition of efficiency in Ref. (Morris and Trivedi, 2007), using  $\hat{k}$  to represent the segment index,  $q_i(t)$  in a unit of  $q_0 = \rho_m v_0$  to denote traffic flow rate at  $x_i$ , and  $u_i(t)$  in unit of  $v_{f2}$  to denote traffic speed at  $x_i$ , the road efficiency at a given time  $t$  and grid  $x_i$ , can be written as

$$\eta(t, x_i) = \frac{\text{Flow}(t) \times \text{Speed}(t)}{\text{Flow}_{\text{Max}} \times \text{Speed}_{\text{Max}}} = \frac{q_i(t) \cdot u_i(t)}{c_r(\hat{k})/e}, \quad (12)$$

where  $c_r(\hat{k})$  is measured by  $v_0 (= \rho_{*2} v_{f2})$ ,  $e = 2.71828$ . Labeling  $s_{1,i} = \rho_1(t, x_i) / [3\rho(t, x_i)]$ ,  $s_{2,i} = \rho_2(t, x_i) / [3\rho(t, x_i)]$ , and  $s_{3,i} = 1 - s_{1,i} - s_{2,i}$ ,  $c_r(\hat{k})$  can be written as

$$c_r(\hat{k}) = \begin{cases} s_{1,i} c_{\tau 1} + s_{2,i} c_{\tau 2} + s_{3,i} c_{\tau 3}, & \text{for } \hat{k} = 3, \\ c_{\tau 4}, & \text{for } \hat{k} = 4. \end{cases} \quad (13)$$

The values for  $c_{\tau j}$ ,  $j = 1, 2, 3, 4$ , used in the numerical simulations have been shown in the second column of Table 1. Therefore, the time-averaged road efficiency at grid  $x_i$  is

$$\eta_{av}(x_i) = \frac{1}{t_{end} - t_{st}} \int_{t_{st}}^{t_{end}} \eta(\xi, x_i) d\xi, \quad (14)$$

with the rms of efficiency given by

$$\eta'(x_i) = \left\{ \frac{1}{t_{end} - t_{st}} \int_{t_{st}}^{t_{end}} [\eta(\xi, x_i) - \eta_{av}(x_i)]^2 d\xi \right\}^{1/2}. \quad (15)$$

It is noted that the grid speed  $u_i(t)$  can also be predicted using more simple traffic model, such as LWR (Lighthill and Whitham, 1955; Richards, 1956). The numerical findings may be not fully the same as that based on the Navier–Stokes like TLM and EZM (see Section 5.2).

**Table 2**  
 $\rho_0$ -dependencies of  $T_{t,av}$ ,  $T_{tu,av}$ ,  $T'_t$  and  $T'_{tu}$  in the case without ramp flow effects for  $v_{f3} = 40$  km/h.

$\rho_0$	TLM				EZM			
	$T_{t,av}$ (h)	$T_{tu,av}$ (h)	$T'_t$ (h)	$T'_{tu}$ (h)	$T_{t,av}$ (h)	$T_{tu,av}$ (h)	$T'_t$ (h)	$T'_{tu}$ (h)
0.1	1.3126	0.1031	0.0049	0.0012	1.3126	0.1032	0.0049	0.0012
0.15	1.5326	0.1230	0.0038	0.0019	1.5328	0.1230	0.0038	0.0017
0.2	1.7686	0.1475	0.0064	0.0037	1.7691	0.1477	0.0065	0.0034
0.25	2.0412	0.1762	0.0058	0.0034	2.0421	0.1763	0.0060	0.0031
0.26	2.1001	0.1832	0.0057	0.0033	2.1010	0.1834	0.0059	0.0034
0.27	2.1600	0.1907	0.0057	0.0041	2.1607	0.1906	0.0058	0.0042
0.28	2.2235	0.2075	0.0070	0.0154	2.2218	0.1983	0.0055	0.0048
0.29	2.2865	0.2156	0.0073	0.0182	2.2880	0.2202	0.0083	0.0220
0.3	2.3558	0.2185	0.0100	0.0183	2.3530	0.2230	0.0089	0.0213
0.368	2.8591	0.2856	0.0253	0.0242	2.8678	0.2853	0.0274	0.0241
0.4	3.1543	0.2849	0.0219	0.0133	3.1451	0.2867	0.0210	0.0152
0.5	4.0651	0.3136	0.0059	0.0059	4.0651	0.3136	0.0059	0.0059

**5. Results and discussion**

**5.1. Simulation parameters**

In the numerical simulations of this paper, it is assumed that the tunnel speed limit is  $v_{f3}(=80$  km/h), the free flow speed on lane I, II are respectively  $v_{f1} = 110$  km/h,  $v_{f2} = 100$  km/h, while the free flow speed on lane III  $v_{f3}$  is selected as 90 km/h, unless the effect of the free flow speed such as  $v_{f3}$  is studied, as shown in Table 1. From the second column of Table 1, it can be seen that the positions of three ramp intersections are respectively  $X_{R1} = 12$  km,  $X_{R2} = 45$  km, and  $X_{R3} = 78$  km. The 3rd column shows that the tunnel entrance is located at  $X_{tu1} = 20$  km, the tunnel length is  $L_{tu} = 8$  km, indicating that the tunnel exit is at  $X_{tu2} = 28$  km. The ring road has a total length  $L = 100$  km, the second critical speed  $u_{c2}$  is 18 km/h, and the relevant Reynolds number  $Re = l_0 v_0 / \nu$  is 64. The parameter to describe the lane changing time is  $\beta_* = 3$ .

To seek tunnel effects on traffic flow on the three lane ring road, as schematically shown in Fig. 2(b), numerical simulations are conducted by solving the equations of TLM, with the FD as shown in Fig. 1. Five initial jams assumed artificially are located at  $X_I$ , ( $I = A, B, C, D, E$ ), other traffic flow parameters, such as the first and second critical densities  $\rho_{*j}$  and  $\rho_{c2j}$ ,  $j = 1, 2, 3, 4$ , are also given in Table 1.

The distribution of initial densities are assumed to be

$$\left. \begin{aligned} \rho_1(0, x) &= \begin{cases} 1, & \text{for } x \in [x_I - 1/2, x_I + 1/2], \\ (1.25 + g_1)\rho_0, & \text{otherwise.} \end{cases} \\ \rho_2(0, x) &= \begin{cases} 1, & \text{for } x \in [x_I - 1/2, x_I + 1/2], \\ (1.25 - g_1)\rho_0, & \text{otherwise.} \end{cases} \\ \rho(0, x) &= \begin{cases} (1 + 1 + \rho_0)/3, & \text{for } x \in [x_I - 1/2, x_I + 1/2], \\ \rho_0, & \text{otherwise.} \end{cases} \end{aligned} \right\} \quad (16)$$

with  $q(0, x) = q_e(\rho(0, x))$ ,  $g_1$  is a random number produced by corresponding generator with Gaussian normal distribution, its average value is 0, and its root mean square (rms) value is set as 0.025. It implies that the initial traffic density on lane III is

$$\rho_3(0, x) = \begin{cases} \rho_0, & \text{for } x \in [x_I - 1/2, x_I + 1/2], \\ \rho_0/2, & \text{otherwise.} \end{cases}$$

The propagation of initial jams is extremely dependent on the value of initial density  $\rho_0$ , tunnel effects, ramp flow effects and the value of  $\gamma$  (Smirnova, et al. 2016, 2017).

**5.2. Model comparison**

To validate the reliability of TLM, the traffic flow model of Zhang (2003) is employed. The extended Zhang's model (EZM) has the equations written as

$$\begin{cases} \rho_t + q_x = \sigma q / l_0, \\ q_t + \{ q^2 / \rho \}_x = R, \\ (\rho_k)_t + (\rho_k u)_x = (\rho - \rho_k) / (\tau \beta_*), \quad \text{for } k = 1, 2. \end{cases} \quad (17)$$

with

$$R = (q_e - q) / \tau - p_x - [(2\beta c_0) \cdot (c/c_0)] u_x + [(2\beta c_0) \cdot (c/c_0) \rho] u_{xx}.$$

These equations are also solved by the WENO5-RK3 scheme as that for the equations of TLM. By making use of the same formulae for traffic pressure and sound speed in TLM, the EZM is also used to estimate the mean travel time and its root mean square (rms) value to provide the counterpart results for comparison. As shown in Table 2, TLM can predicts practically similar travel time as those estimated by the EZM. For instance, in the case of  $\rho_0 = 0.3$ , as seen in the 4th to last line of Table 2, in comparison with the values predicted by EZM, the deviations of  $T_{t,av}$  and  $T_{tu,av}$  are 0.28% and  $-0.45\%$  h respectively, the deviation of  $T'_t$  is 0.11% h, with the deviation of  $T'_{tu}$  equal to  $-0.3\%$  h. The absolute values of the four mentioned deviations are all less than 0.5% h, or 18 s. This allows us to conclude that TLM is reliable.

**5.3. Spatiotemporal evolution of traffic density**

Detailed behavior of a system is generally not reproducible in analyzing queues in transportation systems (Daganzo, 1997). In this study, to produce the queues on the ring road, it is assumed that there are five initial jams, with the tunnel located between the jams initially located at  $X_A$  and  $X_B$ , as shown in Fig. 2.

Traffic flow pattern illustrated by spatiotemporal evolution of  $\rho$  in the case of completely ignoring ramp flow effects, is helpful to judge whether there exists a traffic shock near the tunnel so that tunnel bottleneck effects become more obvious.

In Figs. 4(a-c), the traffic flow patterns for the free flow speed on lane III  $v_{f3} = 40, 50, 60$  km/h are shown. In the left part of Fig. 4(a), when initial density  $\rho_0 = 0.27$ , from the point view of time averaging,  $\rho$  in the tunnel is higher than that in normal road segment. Initial and spontaneously generated jams propagate forward. Traffic shock has not occurred near the tunnel. However as shown in the right part of Fig. 4(a), when  $\rho_0 = 0.28$ , a traffic shock appears at the tunnel exit when  $t \approx 2.4$  h, propagates backward causing an obvious traffic congestion in the tunnel, suggesting that the threshold of shock formation normalized by jam density  $\rho_{th} \approx 0.28$  when  $v_{f3} = 40$  km/h. As shown in Fig. 4(b), when  $v_{f3} = 50$  km/h, one traffic shock originates at the tunnel exit at

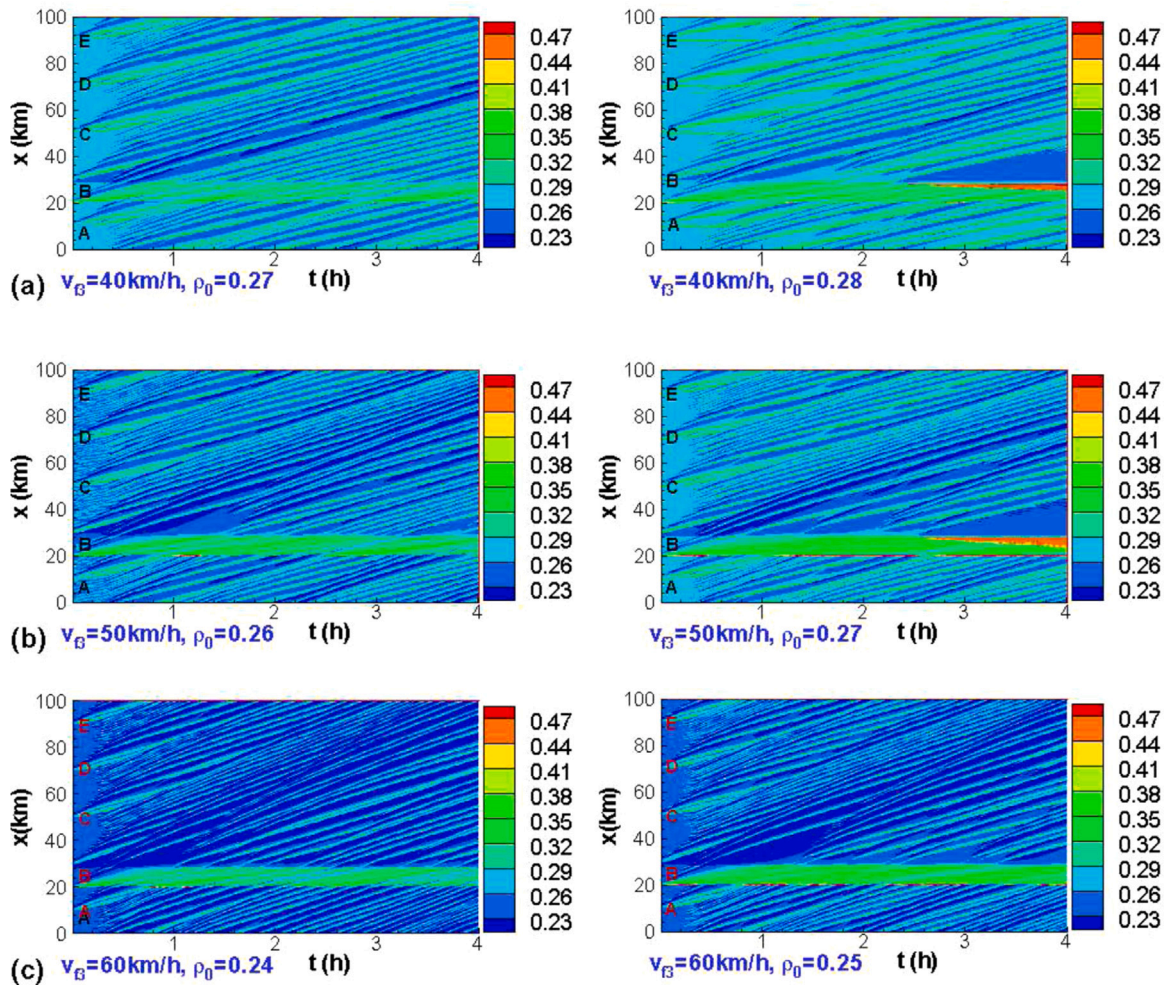


Fig. 4. Spatiotemporal evolution of traffic density  $\rho$  on the ring road in the case without ramp flow effects, (a)  $v_{f3} = 40$  km/h,  $\rho_0 = 0.27$  and 0.28, (b)  $v_{f3} = 50$  km/h,  $\rho_0 = 0.26$  and 0.27, (c)  $v_{f3} = 60$  km/h,  $\rho_0 = 0.24$  and 0.25.

a time of  $t \approx 2.5$  h, another shock at the tunnel entrance appears when  $t \approx 0.15$  h, the normalized threshold of shock formation  $\rho_{th} \approx 0.27$ .

However, when  $v_{f3} = 60$  km/h, there is a traffic shock at tunnel entrance at a time of  $t \approx 0.15$  h,  $\rho_{th} \approx 0.25$ , as can be seen in Fig. 4(c). These traffic flow patterns indicate that the free flow speed on lane III ( $v_{f3}$ ) has a significant effect where and when the tunnel-related traffic shock appears.

Under the conditions ramp flow effects being taken into account, when the mean off-ramp parameter  $\sigma_{2av} = -0.1$ , traffic flow patterns for  $\rho_0 = 0.18$  and 0.19 are shown in Fig. 5(a), where the left part indicates the life time of traffic shock at the tunnel entrance is lower than 0.5 h, while the life time is about 1 h as can be seen in the right part, suggesting that the normalized threshold of shock formation is about 0.19. While the traffic flow patterns shown in Fig. 5(b) indicate the normalized threshold is around 0.2 when the mean off-ramp parameter  $\sigma_{2av} = -0.2$ , suggesting that on-ramp flow has an effect on the value of  $\rho_{th}$ .

The effects of  $v_{f3}$  and the mean off-ramp parameter  $\sigma_{2av}$  on the threshold of traffic shock formation  $\rho_{th}$  can be seen clearly in Table 3. In real freeway networks, the ramp intersections depends on distributions of traffic demands, certainly causing the threshold of traffic shock formation difficult to be measured. Indeed, tunnel bottleneck phenomena are concerned as reported. However, TLM-based numerical finding for threshold  $\rho_{th}$  has an academic significance in understanding the tunnel bottleneck problem.

Note that the traffic flow pattern depends intimately on the evolution of traffic jams and deflation waves and the FD used in numerical

Table 3

Threshold of traffic shock formation.					
Without ramp flow effects, $\sigma_k = 0, k \in [1, 2, 3]$					
$v_{f3}$ (km/h)	40	50	60	70	80
$\rho_{th}$	0.275	0.265	0.245	0.235	0.225
With ramp flow effects, $v_{f3} = 90$ km/h					
$\sigma_{2av}$	-0.1	-0.15	-0.175	-0.2	
$\rho_{th}$	0.185	0.195	0.195	0.195	

simulations, as can be seen in Refs. (Daganzo (1997, Zhang, Wong and Dai, 2009; Lebacque and Khoshyaran 2013; Smirnova, et al. 2017)). TLM has adopted a dynamic FD, as the 1st and 2nd critical densities of the three lane traffic flow are instantaneously determined.

### 5.4. Variable distributions

#### 5.4.1. Instantaneous distributions

The propagation of initial and spontaneously generated jams (Kerner, 1998) can bring about the oscillations of density and speed of traffic flow, depending on the initial density. This explains why the distributions of traffic density and speed at the time of  $t = 1$  h occur oscillations, as shown in Fig. 6(a), where the tunnel with a width 8 km is shown by the solid square. In the segment close to tunnel entrance, the traffic density  $\rho$  is larger, and traffic speed  $u$  is lower inversely as a result of traffic shock formation at tunnel entrance. When  $\rho_0 = 0.25$ , at the time of  $t = 1$  h, in the downstream segment close to tunnel exit,  $\rho$  drops rapidly at first from 0.3 to a value about 0.2 and then gradually

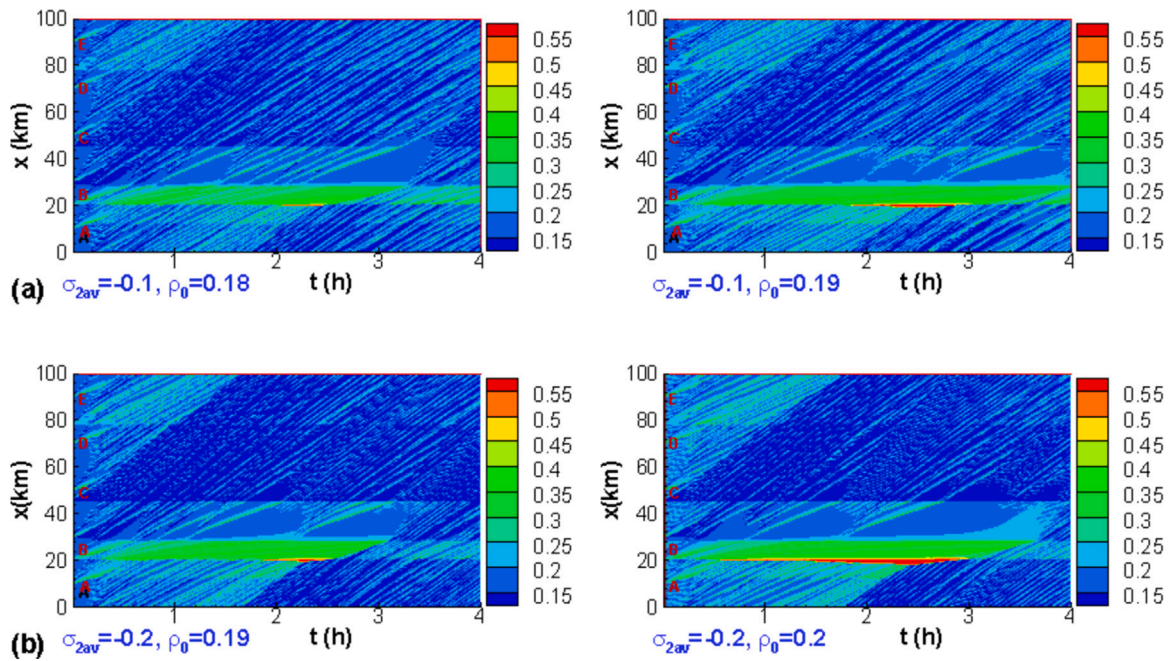


Fig. 5. Spatiotemporal evolution of traffic density  $\rho$  on the ring road in the case with ramp flow effects, (a)  $\sigma_{2av} = -0.1$ ,  $\rho_0 = 0.18$  and  $0.19$ , (b)  $\sigma_{2av} = -0.2$ ,  $\rho_0 = 0.19$  and  $0.2$ .

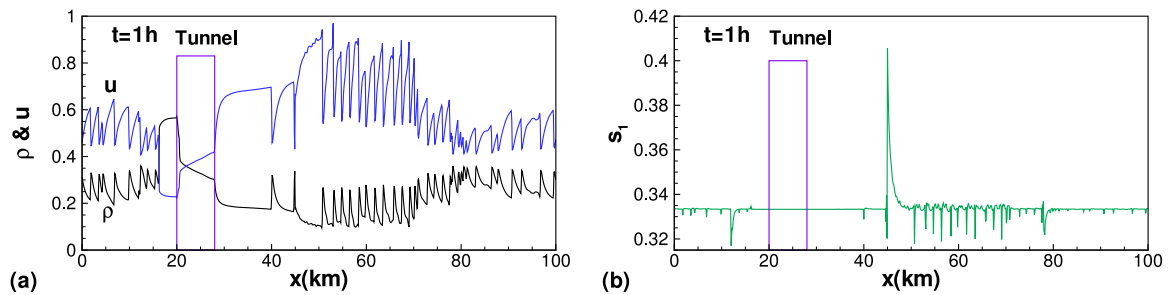


Fig. 6. Distributions of traffic density  $\rho$  and traffic speed  $u$  (a) and density fraction  $s_1 = [\rho_1 / (3\rho)]$  (b) at  $t = 1$  h on the ring road for  $\rho_0 = 0.25$ ,  $\sigma_{av2} = -0.2$ , and  $\sigma_{av1} = \sigma_{av3} = 0.05$ .

decreases to a value of about 0.175 within a distance of about 11 km, indicating that the tunnel provides a smooth downstream segment close to tunnel exit when a traffic shock appears at tunnel entrance.

In Fig. 6(b), the density fraction on lane I  $s_1$  is illustrated. From Eq. , one can derive the equation of  $s_1$

$$\frac{\partial s_1}{\partial t} + u \frac{\partial s_1}{\partial x} = (1/3 - s_1) / (\tau \beta_*) - s \sigma u / l_0.$$

It can be seen that the propagation speed of any disturbance of  $s_1$  is just traffic speed  $u$ , the desired value of  $s_1$  is  $1/3$ . From the source term  $-s_1 \sigma u / l_0$ , it is seen that the on-ramp flows cause two negative pulses at  $X_{R1}$  and  $X_{R2}$ , and the off-ramp flow leads to a positive pulse at  $X_{R2}$ . The ramp shunting at  $X_{R2} = 45$  km plays the role of smoothing segment downstream the ramp intersection.

#### 5.4.2. Time-averaged distributions

For  $\rho_0 = 0.2$  and  $0.368$ , the distributions of  $\eta_{av}$  and  $\eta'$  on the whole ring road in the case accounting for ramp flow effects are presented in Figs. 7(a–b). According to the discussion in sub Section 5.3, when there is ramp flow effects, the threshold for shock formation is about 0.19, implying that for  $\rho_0 = 0.2$ , and  $0.368$ , there is a traffic shock originated at tunnel entrance. From Figs. 7(a–b), it is seen that in the segment from tunnel exit to the intersection at  $X_{R2} = 45$  km, the distributions for  $\eta_{av}$  and  $\eta'$  are almost insensitive to  $\sigma_{2av}$ . Furthermore, for  $\rho_0 = 0.368$ , due to the influence of the propagation of traffic shock, in the segment from the periodic boundary ( $x = 0$ ) to the ramp intersection ( $x = X_{R2}$ ), the

distributions of  $\eta_{av}$  and  $\eta'$  are also almost insensitive to the mean ramp parameter  $\sigma_{2av}$ . The time-averaged road efficiency  $\eta_{av}$  and its rms value  $\eta'$  distribute in a way intimately relying on the choice of  $\rho_0$ . Indeed, the distributions of  $\eta_{av}$  and  $\eta'$  rely on the evolution traffic flow, such as shown in Fig. 5.

#### 5.5. Comparison of results with experimental measurements

For validating TLM, obtained by re-setting the tunnel length as  $L_{tu} = 1.5$  km, the predicted time averaged speed  $u_{av}$  near the tunnel and the corresponding root mean square (rms)  $u'$  for  $\rho_0 = 0.3, 0.368$ , or  $0.4$  in the case for the absence of ramp flow effects are shown in Figs. 8(a–b), with the recorded speed at the Kobotoke tunnel in Japan (Koshi, et al. 1992) and the calculated speed on the basis of a behavioral kinematic wave model (Jin 2018) also illustrated in Fig. 8(a). It can be seen that there is a conformity between  $u_{av}$  and the recorded speed as well as the calculated speed. As the mean travel times through the tunnel with a length of 1.5 km for  $\rho_0 = 0.3, 0.368$ , and  $0.4$  are 0.0541, 0.0545, and 0.0573 h, indicating that the mean traffic speeds through the tunnel are 27.72, 27.52, and 26.178 km/h respectively, which are all in a good agreement with the mean speed 28.9 km/h estimated from the work of Koshi et al.(1992) and the mean speed 33.8 km/h from the work of Jin (2018).

Indeed, this comparison is used just to indicate TLM has its practical reasonability. As reported (Zhang, et al. 2021b), as the traffic flow conditions are naturally different, how much is the uncertainty of the time averaged speed is not crucial.

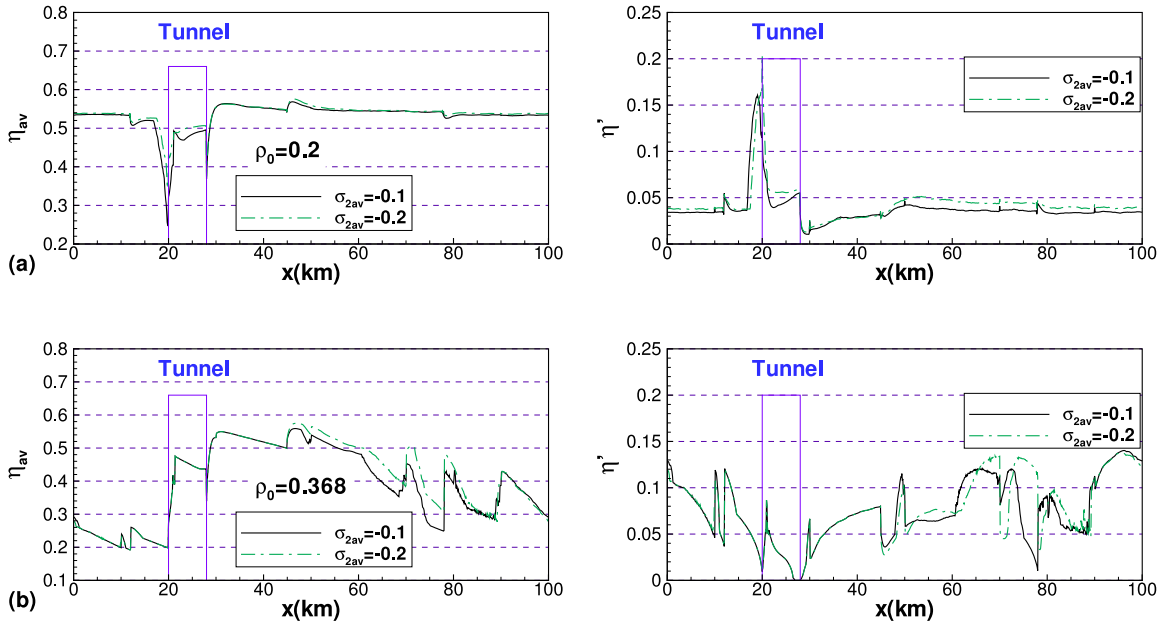


Fig. 7. Distributions of time-averaged road efficiency ( $\eta_{av}$  in left part) and the relevant rms value ( $\eta'$  in right part) on the ring road for (a)  $\rho_0 = 0.2$ , (b)  $\rho_0 = 0.368$ .

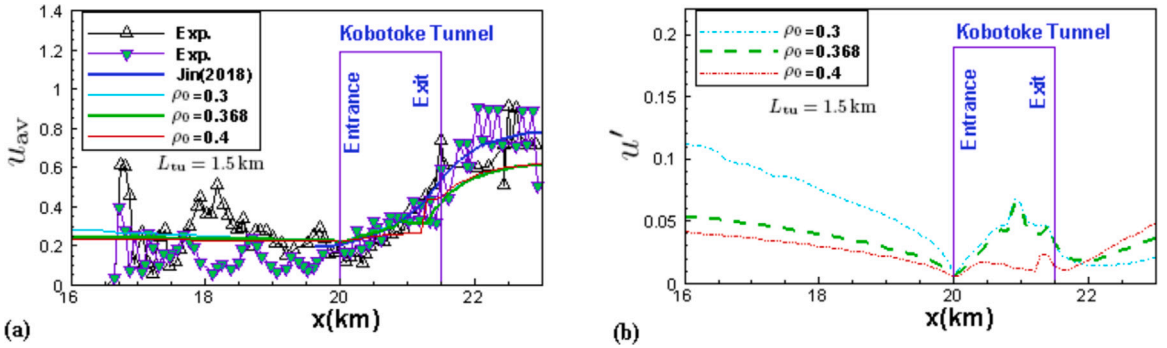


Fig. 8. (a) Comparison of  $u_{av}$  for  $\rho_0 = 0.3, 0.368$ , and  $0.4$  with some existing data, (b) Distribution of rms value  $u'$  near the tunnel. The speed with legend 'Exp.' are recorded at the Kobotoke tunnel in Japan (Koshi, et al. 1992), and the speed shown by the blue solid curve are calculated on the basis of a behavioral kinematic wave model by Jin (2018).

### 5.6. Travel time

Different from the work of Chang and Mahmassani (1988) and Wang et al.(2016), in this paper travel time is calculated using the grid traffic speed  $u_i(t)$  as described in Section 4.1.

Under the conditions ramp flow effects not being taken into account, the  $\rho_0$ - dependencies of the mean travel time  $T_{l,av}$ , its rms  $T'_l$ , the tunnel mean travel time  $T_{tu,av}$ , and its rms  $T'_{tu}$  at different values of  $v_{f3}$  are shown in Figs. 9(a–d). The braking distances for these values of  $v_{f3}$  given in Table 4 are determined by observing whether the FD of traffic on lane III is sufficiently continuous. The data based on TLM labeled by thin solid line with unfilled circles are consistent with the data based on the EZM labeled by red-filled squares excellently. As shown in Fig. 9(a),  $T_{l,av}$  at a given density  $\rho_0$  is shorter when the free flow speed at lane III ( $v_{f3}$ ) is higher. As can be seen in Table 2 and Fig. 9(b), When  $\rho_0$  is below  $\rho_{th}$ ,  $T'_l$  is generally below 0.055.  $T'_l$  is below 0.1 if the initial density is below 0.5 (see Table 4).

The variation of tunnel mean travel time  $T_{tu,av}$  with  $\rho_0$  is illustrated by Fig. 9(c). There exists a turning point on the variation curve of  $T_{tu,av}$ . This point is just at  $\rho_{th}$ . As shown by the curve with green filled circles for  $v_{f3} = 80$  km/h, the turning point is at  $\rho_0 = 0.23$  [see Fig. 5(b)]. The tunnel mean travel time  $T_{tu,av}$  increases with the increase of  $\rho_0$  when  $\rho_0$  varies from 0.1 to 0.22. But as soon as the turning point

Table 4

Braking distances  $X_{br3}$  at different values of  $v_{f3}$ .

$v_{f3}$ (km/h)	40	50	60	70	80
$X_{br3}$ (m)	22.6	29.8	37	44	51

is passed through,  $T_{tu,av}$  quickly approaches to a constant value and shows a plateau in the range from the turning point to the saturation point ( $\rho_0 = 1/e$ ). As seen in Fig. 5,  $\rho_{th}$  relies the value of  $v_{f3}$ , the variation of  $T_{tu,av}$  with  $\rho_0$  depends on the free flow speed on lane III  $v_{f3}$  significantly.

As shown in Fig. 9(d), the dependence of rms  $T'_{tu}$  on  $\rho_0$  has a characteristics that when the density reaches to the turning point, the variation curve of  $T'_{tu}$  has a local peak.

Under the conditions ramp flow effects being taken into account, for the ramp parameters assigned in this study,  $\sum_{k=1}^3 \sigma_{k,av} \leq 0$ , if the sum of  $\sigma_{k,av}$  is negative, ramp flow effects play an overall role of vehicle grooming. Therefore, with the increase of ramp shunting at the intersection  $X_{R2}$ , the mean travel time becomes lower for a given density  $\rho_0$ , as seen in Fig. 10(a). In this work, merely four assignments are tested, by using the linear regression after logarithmic processing (Wang, et al. 1979), an expression for the fitted mean travel

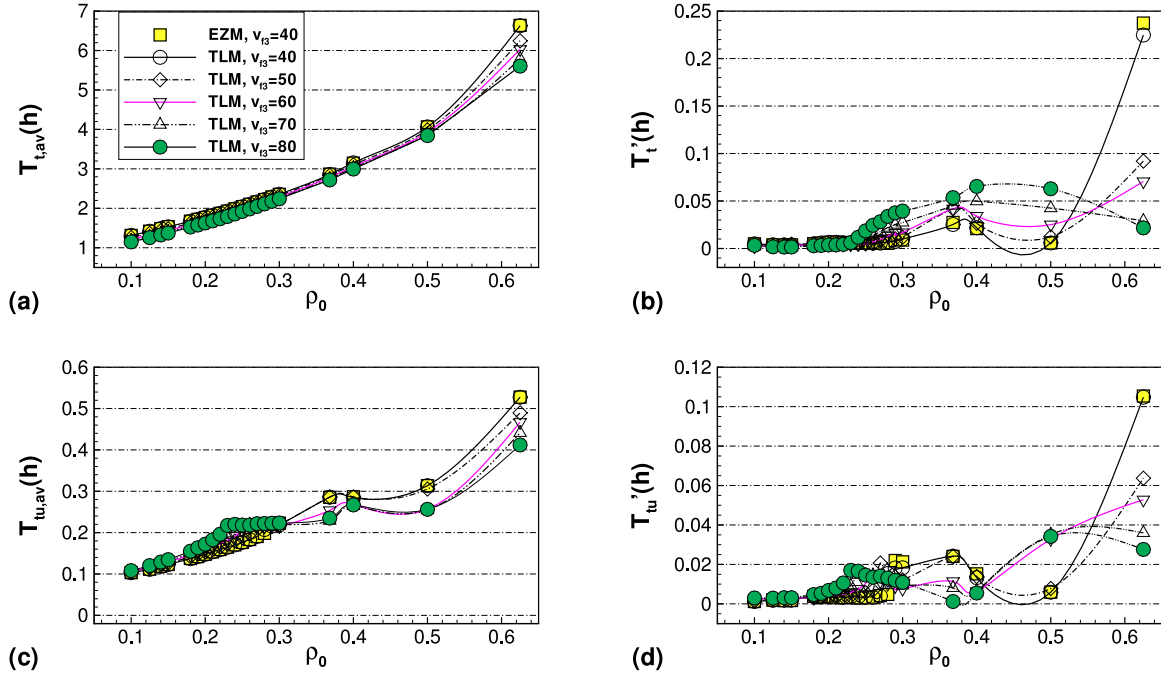


Fig. 9. Density dependencies of (a) mean travel time  $T_{t,av}$ , (b) rms value  $T'_t$ , (c) tunnel mean travel time  $T_{tu,av}$ , and (d) rms value  $T'_{tu}$  in the case without ramp flow effects:  $\sigma_1 = \sigma_2 = \sigma_3 = 0$ .

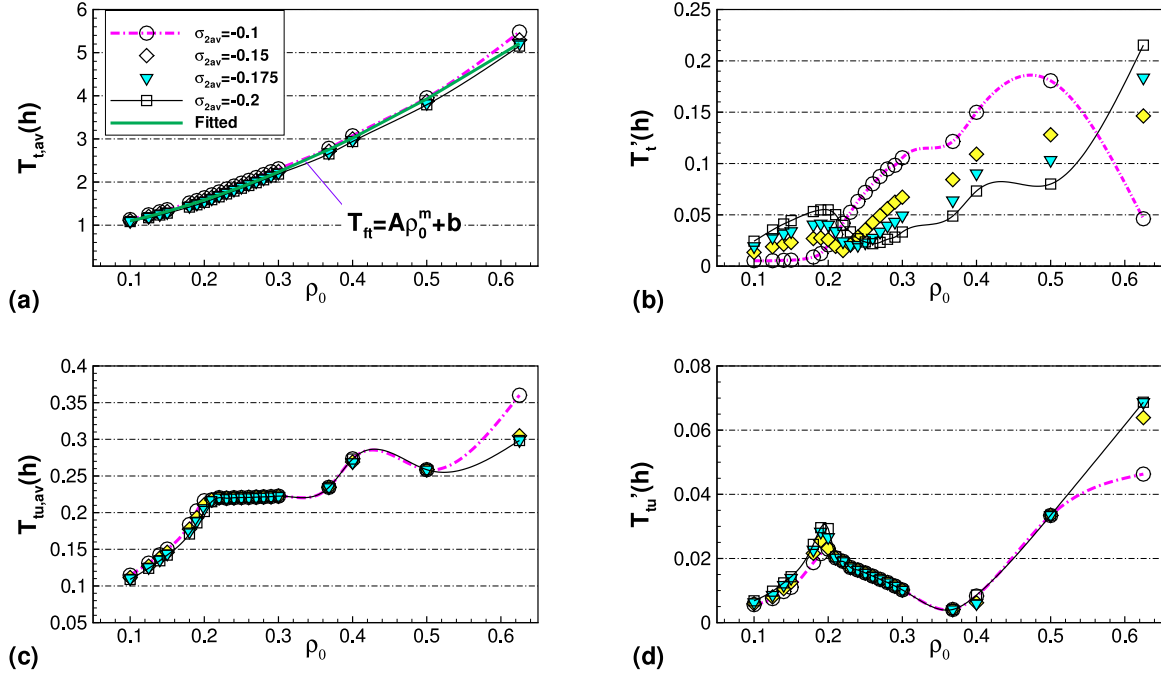


Fig. 10. Density dependencies of (a) mean travel time  $T_{t,av}$ , (b) rms value  $T'_t$ , (c) tunnel mean travel time  $T_{tu,av}$ , and (d) rms value  $T'_{tu}$  for tunnel length  $L_{tu} = 5$  km,  $v_{f3} = 90$  km/h in the case with ramp flow effects. Note that in part (a) of this figure  $A = 9.1060$  h,  $m = 1.5670$ ,  $b = 0.8532$  h.

time  $T_{ft}$  is obtained, its form is

$$T_{ft} = A\rho_0^m + b \tag{18}$$

where  $A = 9.1060$  h,  $m = 1.5670$ ,  $b = 0.8532$  h,  $\rho_0$  ranges from 0.1 to 0.625. The regression of  $\log_{10} A$  and  $m$  has a linear correlation coefficient of 0.9998, with a residual standard deviation of about 0.63%.

As shown in Fig. 10(b), the variation of rms  $T'_t$  with  $\rho_0$  is rather sensitive to the choice of  $\sigma_{2av}$ . In particular, when  $\rho_0$  is assigned below the threshold 0.19,  $T'_t$  is lower, generally below 0.055.

## 6. Conclusions

To ascertain tunnel effects on ring road traffic flow from the view of macroscopic model, a three lane traffic model is proposed. Using the equations of the macroscopic model, a code is elaborated, which allows us to conduct numerical simulations of ring road traffic flow. Numerical results show the following conclusions:

1. The three lane traffic model proposed in this paper can be used in the numerical exploration of tunnel effects upon traffic flow,

which is helpful for deep understanding of the performances of tunnel bottlenecks.

- Under the conditions of ramp flow effects being taken into account, the tunnel generates a shock wave as soon as initial density on the ring road arrives at a threshold. Numerical results from the platform of simulation indicates that the threshold depends on the free flow speed on lane III. When the free flow speed on lane I is 110 km/h, the free flow speed on lane II is 100 km/h, and the tunnel speed limit is 80 km/h, when the free flow speed on lane III is 40 km/h, the threshold in the unit of jam density equals to 0.275, the traffic shock is originated at the tunnel exit; when the free flow speed is 50 km/h, there are two traffic shocks generated by the tunnel, one originates at the tunnel exit, another at the tunnel entrance, the threshold is 0.265; when the free flow speed is 60, 70, or 80 km/h, the traffic shock appears at the tunnel entrance.
- Tunnel provides a smooth downstream segment close to tunnel exit when there is a traffic shock occurs at tunnel entrance. The distributions of mean road efficiency and its root mean square value rely intimately on the spatiotemporal evolution of traffic flow. For instance, when the initial density is equal to the saturation density, a traffic shock originates at tunnel entrance and propagates backward, the interaction and propagation of traffic waves make the distributions of  $\eta_{av}$  and  $\eta'$  in the segment from the periodic boundary ( $x = 0$ ) to the off-ramp intersection almost insensitive to the mean off-ramp parameter.
- In the case with ramp flow effects, the free flow speed on lane III is set as 90 km/h, due to the on-ramp allows vehicles run into the segment upstream the tunnel, the threshold becomes 0.19. The threshold is just the turning point for the variation of tunnel mean travel time with initial density. The tunnel mean travel time increases with the increase of initial density, but when the turning point is passed through, the travel time approaches to a constant quickly and the variation curve show a plateau in the range from the turning point to the saturation point, at which the initial density in the unit of jam density is  $1/e$ . Using linear regression after logarithmic processing, the fitted mean travel time has the form

$$\sigma_{tf} = A\rho_0^m + b$$

where  $A = 9.1060$  h,  $m = 1.5670$ ,  $b = 0.8532$  h,  $\rho_0$  is the initial density in the unit of jam density, has a range from 0.1 to 0.625.

## Nomenclature

<b>A</b>	Jacobian matrix
$B_j$	$= u_{c2}/\{1 - \text{sech}[A_j \ln(\rho_{c2j}/\rho_m)]\}$ , a speed, (km/h)
$c$	traffic sound speed, (m/s)
$c_0$	sound speed at second critical density, (m/s)
$c_{rj}$	equilibrium traffic speed at saturation, $v_0$
$G$	modulus of vehicular fluid elasticity, (veh · m/s <sup>2</sup> )
$l_{veh}$	average vehicle length, (m)
$l_0$	length scale being taken as grid step, (m)
$p$	traffic pressure, (veh · m/s <sup>2</sup> )
$R/\rho$	traffic flow acceleration, (m/s <sup>2</sup> )
$X_{i1}$	position of tunnel entrance (km)
$X_{i2}$	position of tunnel exit (km)
$X_{brj}$	braking distance on lane $j$ for $j = 1, 2, 3$ , in the tunnel for $j = 4$ (m)
$X_{Rk}$	$k$ th ramp intersection
$X_j$	$I = A, B, C, D, E$ , positions of initial traffic jams (km)
$v_{f1}$	free flow speed on lane I, (km/h)
$v_{f2}$	free flow speed on lane II, (km/h)
$v_{f3}$	free flow speed on lane III, (km/h)

## Nomenclature

$v_{f4}$	speed limit of freeway tunnel, (m/s)
$u$	traffic speed, ( $v_{f2}$ )
$u_e$	equilibrium speed, ( $v_{f2}$ )
$v_0$	speed scale, (m/s)
$L$	total length of ring road, (km)
$L_t$	tunnel length, (m)
$\alpha$	$= l\rho_m$
$\beta_*$	ratio of lane-changing time to relaxation time
$\gamma$	traffic flow elasticity, (m <sup>2</sup> )
$\rho$	traffic density, (veh/km)
$\rho_m$	traffic jam density, (veh/km)
$\sigma$	random parameter for ramp flow
$T_{t,av}$	mean travel time, (h)
$T_{tu,av}$	tunnel mean travel time, (h)
$T'_t$	root mean square of travel time, (h)
$T'_{tu}$	root mean square of tunnel travel time, (h)
$\tau$	relaxation time, (s)

## CRediT authorship contribution statement

**Zejing Hu:** Methodology, Software. **M.N. Smirnova:** Conceptualization, Data curation, Writing – original draft. **Yongliang Zhang:** Visualization, Investigation. **Zuojin Zhu:** Validation, Writing – original draft. **N.N. Smirnov:** Supervision, Writing – review & editing.

## Declaration of competing interest

The authors declare that they have no known competing financial interests or personal relationships that could have appeared to influence the work reported in this paper.

## Acknowledgments

We acknowledge the support of National Natural Science Foundation of China (NSFC Grant 11972341) and fundamental research project of Lomonosov Moscow State University ‘Mathematical models for multi-phase media and wave processes in natural, technical and social systems’. We thank Professor Gong Li at USTC and Dr. Y.L. Li at Peking University for some useful private communications.

## References

- Bogdanova, A., Smirnova, M.N., Zhu, Z.J., Smirnov, N.N., 2015. Exploring peculiarities of traffic flows with a viscoelastic model. *Transp. A: Trans. Sci.* 11 (7), 561–578.
- Chang, G.L., Mahmassani, H.S., 1988. Travel time prediction and departure time adjustment behavior dynamics in a congested traffic system. *Transp. Res. Part B: Methodol.* 22 (2), 217–232.
- Chang, G.L., Zhu, Z.J., 2006. A macroscopic traffic model for highway work zones: formulations and numerical results. *J. Adv. Transp.* 40 (3), 265–287.
- Chen, C., Jia, Z., Varaiya, O., 2001. Causes and cures of highway congestion. *IEEE Control Syst. Mag.* 21 (6), 26–32.
- Daganzo, C., 1997. Traffic flow theory. In: Daganzo, C. (Ed.), *Fundamentals of Transportation and Traffic Operations*. Pergamon, New York, pp. 67–160.
- Daganzo, C., 2002a. A behavioral theory of multi-lane traffic flow: Part I: Long homogeneous freeway sections. *Transp. Res. Part B: Methodol.* 36, 131–158.
- Daganzo, C., 2002b. A behavioral theory of multi-lane traffic flow: Part II: Merges and onset of congestion. *Transp. Res. Part B: Methodol.* 36, 159–169.
- Gofii-Ros, B., Knoop, V.L., van Arem, B., Hoogendoorn, S.P., 2014. Mainstream traffic flow control at sags. *Transp. Res. Rec.: J. Transp. Res. Board* 2470 (1), 57–64.
- Gofii-Ros, B., Knoop, V.L., Takahashi, T., Sakata, I., van Arem, B., Hoogendoorn, S.P., 2016. Optimization of traffic flow at freeway sags by controlling the acceleration of vehicles equipped with in-car systems. *Transp. Res. Part C: Emerg. Technol.* 71, 1–18.
- Haight, F., 1963. *Mathematical Theories of Traffic Flow*. Academic Press, New York.
- Helbing, D., 2001. Traffic and related self-driven many-particle systems. *Rev. Modern Phys.* 73 (4), 1067–1414.
- Helbing, D., Greiner, A., 1997. Modeling and simulation of multilane traffic flow. *Phys. Rev. E* 55 (5), 5498–5508.
- Helbing, D., Treiber, M., 1998. Gas-kinetic-based traffic model explaining observed hysteretic phase transition. *Phys. Rev. Lett.* 81, 3042–3045.

- Henrick, A.K., Aslam, T.D., Powers, J.M., 2005. Mapped weighted essentially non-oscillatory schemes: Achieving optimal order near critical points. *J. Comput. Phys.* 207, 542–567.
- Hoogendoorn, S.P., Bovy, P.H.L., 2000. Continuum modeling of multiclass traffic flow. *Transp. Res. Part B: Methodol.* 34 (2), 123–146.
- Jiang, G.S., Shu, C.W., 1996. Efficient implementation of weighted ENO schemes. *J. Comput. Phys.* 126, 202–228.
- Jin, W.L., 2018. Kinematic wave models of sag and tunnel bottlenecks. *Transp. Res. Part B: Methodol.* 107, 41–56.
- Kerner, B., 1998. Experimental features of self-organization in traffic flow. *Phys. Rev. Lett.* 81 (17), 3797–3800.
- Kiselev, A.B., Nikitin, N.F., Smirnov, N.N., Yumashev, M.V., 2000. Irregular traffic flow on a ring road. *J. Appl. Math. Mech.* 64 (4), 627–634.
- Koshi, M., Kuwahara, M., Akahane, H., 1992. Capacity of sags and tunnels on Japanese motorways. *ITE J.* 62 (5), 17–22.
- Lebacque, J.P., Khoshyaran, M.M., 2013. A variational formulation for higher order macroscopic traffic flow models of the GSOM family. *Transp. Res. Part B: Methodol.* 57, 245–265.
- Lighthill, M.J., Whitham, G.B., 1955. On kinematic waves II: a theory of traffic flow on long crowded roads. *Proc. Roy. Soc. Lond A* 229, 317–345.
- Ma, J., Chan, C.K., Ye, Z.B., Zhu, Z.J., 2018. Effects of maximum relaxation in viscoelastic traffic flow modeling. *Transp. Res. Part B: Methodol.* 113, 143–163.
- Michalopoulos, P.G., Beskos, D.E., Yamauchi, Y., 1984. Multilane traffic flow dynamics: Some macroscopic considerations. *Transp. Res. Part B: Methodol.* 18 (4-5), 377–395.
- Morris, B., Trivedi, M., 2007. Real-time video based highway traffic measurement and performance monitoring. In: 2007 IEEE Intelligent Transportation Systems Conference. IEEE, Sept. 30 - Oct. 3, Seattle, WA, USA.
- Richards, P., 1956. Shock waves on the freeway. *Oper. Res.* 4, 42–51.
- Shu, C.W., 1988. Total-variation-diminishing time discretizations. *SIAM J. Sci. Stat. Comput.* 9, 1073–1084.
- Shu, C.W., Osher, S., 1989. Efficient implementation of essentially non-oscillatory shock-capturing schemes. *J. Comput. Phys.* 83, 32–78.
- Shui, H., 1998. TVD scheme. In: Shui, H. (Ed.), *Finite Difference in One-Dimensional Fluid Mechanics*. Beijing, in Chinese, National Defense, pp. 333–355.
- Smirnova, M.N., Bogdanova, A.I., Smirnov, N.N., Kiselev, A.B., Nikitin, N.F., Manenkova, A.S., 2014b. Multi-lane unsteady-state traffic flow models. *J. Mechatron.* 2 (4), 1–5.
- Smirnova, M.N., Bogdanova, A.I., Zhu, Z.J., Smirnov, N.N., 2016. Traffic flow sensitivity to visco-elasticity. *Theor. Appl. Mech. Lett.* 6, 182–185.
- Smirnova, M.N., Bogdanova, A.I., Zhu, Z.J., Smirnov, N.N., 2017. Traffic flow sensitivity to parameters in viscoelastic modelling. *Transportmetrica B: Transp. Dynam.* 5 (1), 115–131.
- Wang, L.X., Fang, D.Z., et al., 1979. Regression analysis. In: Wang, Y., Wan, Z.X. (Eds.), *Handbook of Mathematics*. Higher Education Press, Beijing, in Chinese, pp. 836–847.
- Wang, D.H., Fu, F.J., Luo, X.Q., Jin, S., Ma, D.F., 2016. Travel time estimation method for urban road based on traffic stream directions. *Transportmetrica A: Transp. Sci.* 12 (6), 497–503.
- Zhang, H., 2003. Driver memory, traffic viscosity and a viscous vehicular traffic flow model. *Transp. Res. Part B: Methodol.* 37, 27–41.
- Zhang, Y.L., Smirnova, M.N., Bogdanova, A.I., Zhu, Z.J., Smirnov, N.N., 2018a. Travel time estimation by urgent-gentle class traffic flow model. *Transp. Res. Part B: Methodol.* 113, 121–142.
- Zhang, Y.L., Smirnova, M.N., Bogdanova, A.I., Zhu, Z.J., Smirnov, N.N., 2018b. Travel time prediction with a viscoelastic traffic model. *Appl. Math. Mech. (English Edition)* 39 (12), 1769–1788.
- Zhang, Y.L., Smirnova, M.N., Ma, J., Smirnov, N.N., Zhu, Z.J., 2021a. Freeway tunnel effect of travel time based-on a double lane traffic model. *Int. J. Transp. Sci. Technol.* <http://dx.doi.org/10.1016/j.ijst.2021.05.002>, (in press) 6 May 2021.
- Zhang, Y.L., Smirnova, M.N., Ma, J., Smirnov, N.N., Zhu, Z.J., 2021b. Tunnel effects on ring road traffic flow based on an urgent-gentle class traffic model. *Theor. Appl. Mech. Lett.* 11 (4), 100283. <http://dx.doi.org/10.1016/j.taml.2021.100283>.
- Zhang, P., Wong, S.C., Dai, S.Q., 2009. A conserved higher order aniso-tropic traffic flow model: Description of equilibrium and non-equilibrium flows. *Transp. Res. Part B: Methodol.* 43 (5), 562–574.
- Zhu, Z.J., Yang, C., 2013. Visco-elastic traffic flow model. *J. Adv. Transp.* 47, 635–649.